Langmuir
Article
pubs.acs.org/Langmuir

Droplet Evaporation of Pure Water and Protein Solution on Nanostructured Superhydrophobic Surfaces of Varying Heights

Chang-Hwan Choi*,† and Chang-Jin "CJ" Kim‡

†Department of Mechanical Engineering, Stevens Institute of Technology, Hoboken, New Jersey 07030, and ‡Mechanical and Aerospace Engineering Department, University of California at Los Angeles (UCLA), Los Angeles, California 90095

Received October 31, 2008. Revised Manuscript Received May 4, 2009

Evaporation of liquids on substrates is important for many applications including lab-on-a-chip, especially when they are in droplets. Unlike on planar substrates, droplet evaporation on micropatterned substrates has been studied only recently and none so far on nanopatterns. Driven by the applicability of nanostructured surfaces to biomaterials and tissue engineering, we report on the evaporative process of sessile droplets of pure water and a protein solution on superhydrophobic surfaces of sharp-tip post structures in a submicrometer pitch (230 nm) and varying heights (100−500 nm). We find that the nanotopographical three-dimensionalities such as structural height and sidewall profile affect the surface superhydrophobicity in such a way that only tall and slender nanostructures provide the surface with great superhydrophobicity (a contact angle more than 170°). The evaporation process was different between the pure water and the protein solution; unlike pure water, a significant contact-line spreading and pinning effect was observed in a droplet of a protein solution with an intermediate transition from a dewetting (Cassie) to a wetting (Wenzel) state. Enabled by well-defined nanostructures, our results highlight that the surface superhydrophobicity and the droplet evaporation are significantly affected by the three-dimensional nanometric topography and the surface fouling such as protein adsorption.

1. Introduction

Surface superhydrophobicity, endowed by hydrophobic micro- or nanoscale surface patterns, has long been utilized in many natural surfaces such as insect wings and lotus leaves for their self-cleaning mechanism due to its high water repellency.[1,2] Such highly nonwetting superhydrophobic surfaces[3−5] have recently drawn much attention for engineering applications such as friction reduction in continuous flows[6−9] or droplet driving in microfluidic systems.[10,11] While most reports using well-defined surface structures had microscale patterns,[6,9] a few had nanoscale patterns to resist better against the transition to wetting.[7,8]

Surface wettability also affects the evaporation of liquids, which is pronounced in the microscale and thus important for microfluidic applications. For example, the evaporative processes of droplets on solid surfaces are critical for applications such as inkjet printing,[12,13] spraying,[14,15] DNA chip,[16,17] and MALDI-MS (matrix-assisted laser desorption/ionization mass spectrometry).[18,19] Although the studies on the evaporation on common (e.g., planar) hydrophilic or hydrophobic surfaces have been extensive, the investigations on patterned hydrophobic surfaces (i.e., superhydrophobic surfaces) have started only recently.[20−26] Furthermore, the studied surface patterns were either of microscale,[20−23] limiting the range of study only down to ∼0.1 mm in droplet size as it shrinks, or randomly roughened,[24−26] not allowing a systematic study on surface parameters such as structural spacing, height, and shape. Additionally, the tested liquids were mostly pure water.[20−25] It has not been studied how droplets of complex fluids (e.g., suspensions of nanoparticles such as DNA or proteins in a base fluid) would evaporate on the structured surfaces.

*Corresponding author. E-mail: cchoi@stevens.edu. Tel.: +1 201 216 5579. Fax: +1 201 216 8315.

(1) Wagner, T.; Neinhuis, C.; Barthlott, W. *Acta Zool.* **1996**, *77*, 213−225.
(2) Barthlott, W.; Neinhuis, C. *Planta* **1997**, *202*, 1−8.
(3) Nakajima, A.; Hashimoto, K.; Watanabe, T. *Monatsh. Chem.* **2001**, *132*, 31−41.
(4) Blossey, R. *Nat. Mater.* **2003**, *2*, 301−306.
(5) Quere, D. *Rep. Prog. Phys.* **2005**, *68*, 2495−2532.
(6) Ou, J.; Perot, B.; Rothstein, J. P. *Phys. Fluids* **2004**, *16*, 4635−4643.
(7) Choi, C.-H.; Ulmanella, U.; Kim, J.; Ho, C.-M.; Kim, C.-J. *Phys. Fluids* **2006**, *18*, 087105.
(8) Choi, C.-H.; Kim, C.-J. *Phys. Rev. Lett.* **2006**, *96*, 066001.
(9) Lee, C.; Choi, C.-H.; Kim, C.-J. *Phys. Rev. Lett.* **2008**, *101*, 064501.
(10) Kim, J.; Kim, C.-J., Nanostructured surfaces for dramatic reduction of flow resistance in droplet-based microfluidics. In *Proceeding of the 15th IEEE International Conference on Micro Electro Mechanical System*; IEEE: Las Vegas, NV, USA, 2002; pp 479−482.
(11) Yun, K.-S.; Kim, C.-J. Low-voltage electrostatic actuation of droplet on thin superhydrophobic nanoturf. In *Proceeding of the 20th IEEE International Conference on Micro Electro Mechanical Systems*; IEEE: Kobe, Japan, 2007; pp 139−142.
(12) Le, H. P. *J. Imaging Sci. Technol.* **1998**, *42*, 49−62.
(13) Calvert, P. *Chem. Mater.* **2001**, *13*, 3299−3305.
(14) Bruinsma, P. J.; Kim, A. Y.; Liu, J.; Baskaran, S. *Chem. Mater.* **1997**, *9*, 2507−2512.
(15) Rietveld, I. B.; Kobayashi, K.; Yamada, H.; Matsushige, K. *J. Phys. Chem. B* **2006**, *110*, 23351−23364.
(16) Dugas, V.; Broutin, J.; Souteyrand, E. *Langmuir* **2005**, *21*, 9130−9136.
(17) Fang, X.; Li, B.; Petersen, E.; Seo, Y.-S.; Samuilov, V. A.; Chen, Y.; Sokolov, J. C.; Shew, C.-Y.; Rafailovich, M. H. *Langmuir* **2006**, *22*, 6308−6312.
(18) Schuerenberg, M.; Luebbert, C.; Eickhoff, H.; Kalkum, M.; Lehrach, H.; Nordhoff, E. *Anal. Chem.* **2000**, *72*, 3436−3442.
(19) Moon, H.; Wheeler, A. R.; Garrell, R. L.; Loo, J. A.; Kim, C.-J. *Lab Chip* **2006**, *6*, 1213−1219.
(20) McHale, G.; Aqil, S.; Shirtcliffe, N. J.; Newton, M. I.; Erbil, H. Y. *Langmuir* **2005**, *21*, 11053−11060.
(21) Bartolo, D.; Bouamrirene, F.; Verneuil, E.; Buguin, A.; Silberzan, P.; Moulinet, S. *Eur. Phys. Lett.* **2006**, *74*, 299−305.
(22) Jung, Y. C.; Bhushan, B. *J. Microsc.* **2008**, *229*, 127−140.
(23) Reyssat, M.; Yeomans, J. M.; Quere, D. *Eur. Phys. Lett.* **2008**, *81*, 26006.
(24) Zhang, X.; Tan, S.; Zhao, N.; Guo, X.; Zhang, X.; Zhang, Y.; Xu, J. *ChemPhysChem* **2006**, *7*, 2067−2070.
(25) Bormashenko, E.; Bormashenko, Y.; Stein, T.; Whyman, G.; Pogreb, R. *Langmuir* **2007**, *23*, 4378−4382.
(26) McLauchlin, M. L.; Yang, D.; Aella, P.; A., G. A.; Picraus, S. T.; Hayes, M. A. *Langmuir* **2007**, *23*, 4871−4877.

This paper is an experimental investigation of droplet evaporation on the superhydrophobic surfaces of well-regulated nanostructures. The surfaces are covered with needle-like sharp-tip post structures in a fixed nanometric pitch (periodicity) but varying heights. Motivated by the recent investigation on the cell interactions with the nanostructured surface,[27,28] two different liquids—pure water and a protein solution of cell culture media—are tested on such well-controlled nanotopographical surfaces to examine the effect of the biological complex fluids on the surface superhydrophobicity and droplet evaporation.

2. Theoretical Background

Dewetting Superhydrophobic Surface Condition. Surface parameters such as structural pitch, height, and sidewall profile affect the hydrophobicity of superhydrophobic surfaces. The condition to sustain a liquid−air interface against a differential liquid pressure can be analyzed by minimizing the free energy of the interface[29] or by the force balance between the pressure across the interface and its tension.[30] For the sharp-tip nanopost structures considered in this paper (Figure 1a), the criterion to maintain the dewetted state can be reduced to the following equations:

$$p < \sqrt{\frac{\pi d^2}{4} - \frac{\pi\gamma d\cos(\theta_A - \alpha)}{\Delta P}} \cong \sqrt{-\frac{\pi\gamma d\cos(\theta_A - \alpha)}{\Delta P}} \quad (\text{if } d \ll p) \tag{1}$$

$$h > \frac{1-\sin(\theta_A - \alpha)}{-2\cos(\theta_A - \alpha)}(\sqrt{2}p - d) \cong \frac{1-\sin(\theta_A - \alpha)}{-\sqrt{2}\cos(\theta_A - \alpha)}p \quad (\text{if } d \ll p) \tag{2}$$

where p = structural pitch, d = tip diameter, γ = liquid−air interfacial tension, θ_A = advancing contact angle, α = cone angle, ΔP = liquid pressure over air (i.e., $P_l - P_a$), and h = structural height. Figure 1b,c shows a maximally allowable pitch and a minimally required height for the sharp-tip ($d \ll p$) post patterns to sustain the liquid meniscus, with water (γ = 72.7 mN/m at 20 °C) as a liquid. Note that hydrostatic pressure is negligible for a small droplet, but Laplace pressure by its tight curvature is significant. For example, $\Delta P = 2\gamma/R$ for a spherical droplet of radius R; while $\Delta P \cong 150$ Pa for a water droplet of R = 1 mm and $\Delta P \cong 0.15$ MPa for a droplet of R = 1 μm. If liquid pressure gets larger than the maximally allowable pressure at a given pitch, the surface tension cannot withstand the pressure force, and the liquid meniscus will slide (or advance) down along the sides of the post structures. If the liquid touches the bottom surface and replaces the air, the surface will lose its superhydrophobicity by homogeneous wetting. It should be noted that, even for the highly hydrophobic materials such as Teflon, the advancing contact angle θ_A of water on the flat surface is not more than ~130°, suggesting that a structural pitch in submicrometer is desirable in order to sustain a relatively high pressure (e.g., near atmospheric pressure) (Figure 1b). It should also be noted that slender structures with a smaller (or even negative) slope angle α are more desirable to support a higher pressure at a given pitch. In addition, the structures should be tall enough (Figure 1c); if not, the warping liquid meniscus due to a pressure will touch the bottom surface even before the contact line starts to slide down from the tip. Thus, the key geometrical requirements for the dewetted superhydrophobic surface state is to have tall and slender (i.e., high-aspect-ratio), dense-array (e.g., submicrometer-pitch) nanostructures.

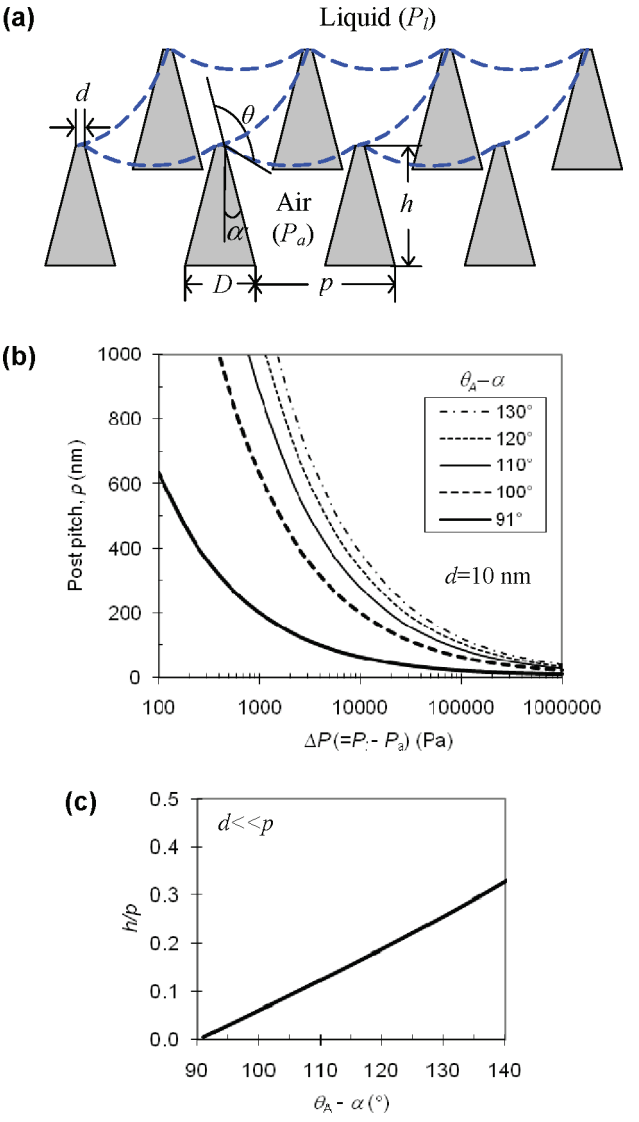

Figure 1. Geometric requirements to maintain a dewetted (Cassie) superhydrophobic state: (a) Liquid meniscus expected over hydrophobic post structures. A square-array post pattern has periodicity (pitch) p, height h, base diameter D, tip diameter d, and cone angle (or slope) α. A liquid meniscus is assumed to have a spherical shape, forming contact angle θ with post side in the case of $d \ll p$. If liquid pressure P_l increases against air pressure P_a, more than the amount a surface tension of the curved meniscus can balance, the meniscus would slide down with advancing contact angle θ_A and fill the space between structures, causing a loss of superhydrophobicity. (b) Maximum pitch p allowable to hold a pressurized water meniscus over posts with tip diameter d = 10 nm. (c) Minimum height-to-pitch ratio required for a warping water meniscus not to touch the bottom surface in case of $d \ll p$.

Contact Angle on a Superhydrophobic Surface. The surface superhydrophobicity is typically examined by measuring a contact angle of a sessile drop. For a dewetted (Cassie) state, a theoretical contact angle follows the Cassie−Baxter equation:[31]

$$\cos\theta = f_{SL}\cos\theta_0 - 1 + f_{SL} \tag{3}$$

(27) Choi, C.-H.; Hagvall, S. H.; Wu, B. M.; Dunn, J. C. Y.; Beygui, R. E.; Kim, C.-J. *Biomaterials* **2007**, *28*, 1672−1679.
(28) Choi, C.-H.; Hagvall, S. H.; Wu, B. M.; Dunn, J. C. Y.; Beygui, R. E.; Kim, C.-J. *J. Biomed. Mater. Res., Part A* **2009**, *89*, 804−817.
(29) Extrand, C. W. *Langmuir* **2004**, *20*, 5013−5018.
(30) Zheng, Q.-S.; Yu, Y.; Zhao, Z.-H. *Langmuir* **2005**, *21*, 12207−12212.
(31) Cassie, A. B. D.; Baxter, S. *Trans. Faraday Soc.* **1944**, *40*, 546−551.

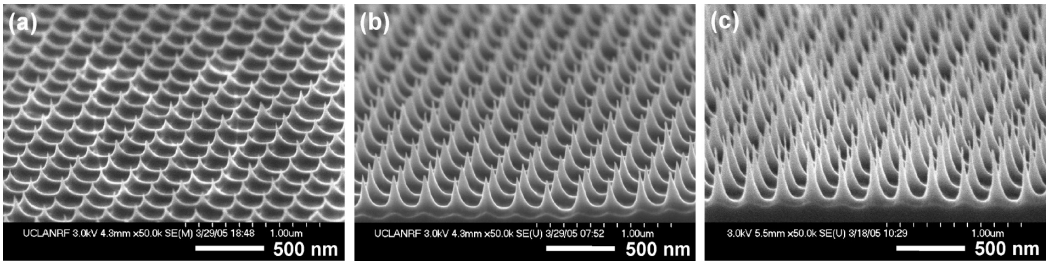

Figure 2. SEM images (tilted views) of sharp-tip nanopost structures on three types of samples tested: (a) Nanopost-Low, (b) Nanopost-Mid, and (c) Nanopost-High. Well-ordered dense-array silicon nanopost structures covered a sample surface uniformly (less than 10% deviation in a structural height in 1×1 cm^2). While pattern periodicity was maintained to be 230 nm and structural tips were all sharpened to be less than 10 nm in a tip apex radius of curvature, only structural heights were varied from ~100 nm (a), ~300 nm (b), to ~500 nm (c).

where θ denotes an apparent contact angle on a composite interface of solid and gas, f_{SL} a fraction of wet surface (i.e., solid−liquid fraction), and θ_0 a contact angle on a referential smooth surface. If liquid wets the surface (Wenzel state), a theoretical contact angle follows the Wenzel equation:[32]

$$\cos\theta = R_f \cos\theta_0 \tag{4}$$

where θ denotes an apparent contact angle on a homogeneously rough surface, R_f a surface roughness factor defined as the ratio of the actual surface area to its flat projection, and θ_0 a contact angle on a referential smooth surface. For the sharp-tip nanopost structures shown in Figure 1a, f_{SL} and R_f are estimated as

$$f_{SL} = \frac{\pi d^2}{4p^2} \tag{5}$$

$$R_f = 1 + \frac{\pi(\sqrt{1 + 4h^2/D^2} - 1)}{4P^2/D^2} \tag{6}$$

where it is assumed that $d \ll p$ in deriving eq 6.

3. Experimental Approach

Surface Samples. Figure 2 shows the scanning electron microscope (SEM) images of the sharp-tip nanopost structures of varying heights, whose fabrication procedure has been reported elsewhere.[33] The well-ordered, dense-square-array silicon nanopost structures were created uniformly over the top surface of the sample (1×1 cm^2). While the pattern periodicity was maintained to be 230 nm, the structure height was controlled from "Low" (~100 nm), "Mid" (~300 nm), to "High" (~500 nm) to represent varying nanotopographical three-dimensionality. SEM images taken at multiple points along the cross sections of the samples determined that the deviation of structural height for each sample was less than 10%. The deviation will not affect the theoretical contact angle at a dewetted state, while it creates error in a wetted state contact angle, e.g., ± 2° for the Low (~100 nm high) sample. To maximize the surface superhydrophobicity (i.e., to minimize the solid−liquid fraction in case of the Cassie state), structural tips were all sharpened to be needle-like (the tip apex radius of curvature ~10 nm). Planar silicon samples (1×1 cm^2) of a polished smooth surface were also prepared as controls. Each sample was then coated with Teflon (~10 nm thick) to make the surfaces hydrophobic.

Test Liquids. For water, purified deionized (DI) water was tested. For a protein solution, a cell culture medium of Dulbecco's Modified Eagle's Medium (DMEM) (Invitrogen) was tested.

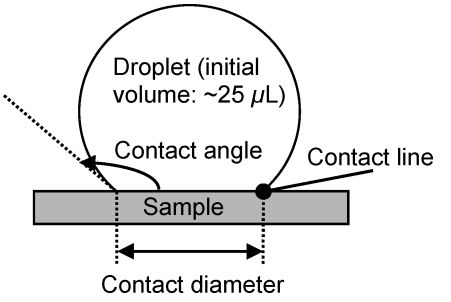

Figure 3. Schematic of an evaporating droplet on a sample.

DMEM contains various amino acids and vitamins, supplemented with 10% fetal bovine serum (Invitrogen) and 100 U/mL penicillin/streptomycin (Invitrogen).

Measurement of Contact Angles and Contact Diameters. Contact angles and contact diameters of evaporating liquid droplets on samples were measured by using a contact angle analyzer (FTA4000, First Ten Angstroms Inc., Portsmouth, VA). All four samples (Smooth, Nanopost-Low, -Mid, and -High) were placed together on a sample stage to ensure uniform environmental conditions such as temperature and humidity during a test. A droplet (initial volume: ~25 μL) of a test liquid was dispensed on each sample by a micropipet. Droplets were left to evaporate in room condition. The images of evaporating droplets were captured by every 10−20 min using an analytical microscope and camera until the samples were dried out. The contact angles and contact diameters of the evaporating droplets, as defined in Figure 3, were measured from a series of captured images. The experiments were performed three times for both water and DMEM.

4. Results and Discussion

Evaporation of a Water Droplet. Figure 4 is a set (i.e., one of the three repeated tests) of the captured images of water droplets during the evaporation. From all three sets of the captured images, the contact angle and the contact diameter of the evaporating droplets were measured, as presented in Figure 5.

On Smooth (● in Figure 5), for the beginning 30 min, the initial contact angle (~116°) continuously decreased down to ~110° (Figure 5a) with a slight decrease of a contact diameter (Figure 5b). Then, the contact line retreated with an almost constant receding contact angle (110 ± 2°) with a continual decrease of a contact diameter until dryout (Figure 5c).

On Nanopost-Low (□ in Figure 5), a contact angle started at a little bit higher value (~133°) than that on Smooth (Figure 5a). On the basis of the geometrical dimensions measured from the image (Figure 2a) and the estimated Teflon coating thickness (~10 nm) uniform over the surface, a solid−liquid fraction f_{SL} and a surface roughness factor R_f estimated for the Cassie and Wenzel states are 0.013 and 1.28, respectively. If the initial contact

(32) Wenzel, R. *Ind. Eng. Chem.* **1936**, *28*, 988−994.
(33) Choi, C.-H.; Kim, C.-J. *Nanotechnology* **2006**, *17*, 5326−5333.

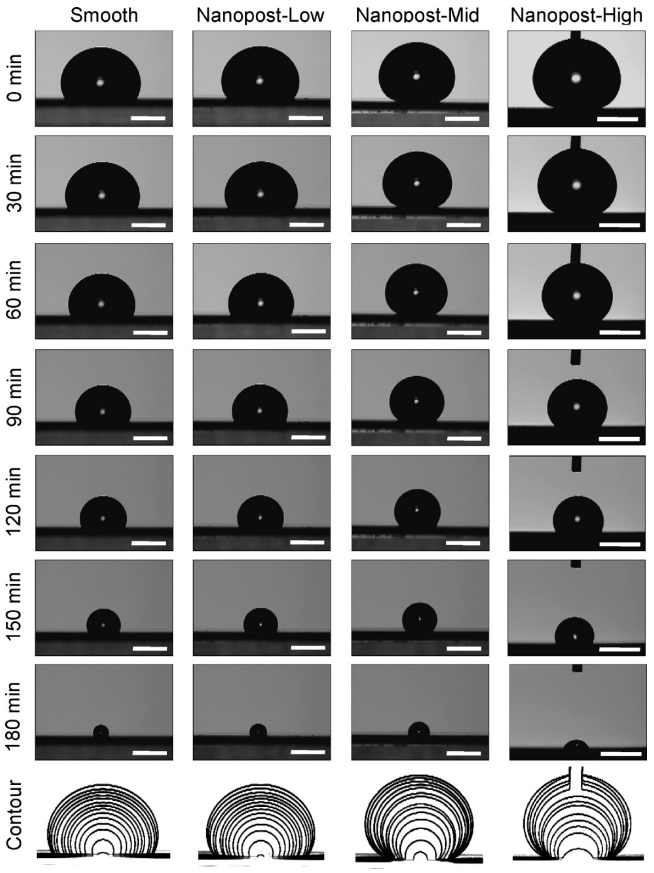

Figure 4. Evaporation of water droplets. Images of droplets (initial volume of ~25 μL) were taken over time in a room environment on smooth and nanopost samples. From the images, the evolution of a contact angle and a contact diameter were measured. The images are shown here for every 30 min. Each scale bar indicates 1 mm. Contours of the droplets were captured by image analysis and drawn overlapping to show the evolution. The vertical pin in Nanopost-High pictures was used to keep the droplet in position against rolling away.

angle (116°) on Smooth is used as a referential contact angle θ_0, a theoretical contact angle estimated by the Cassie and Wenzel equations are 173° and 124°, respectively. Although the initial contact angle on the Nanopost-Low (~133°) was a little bit larger than the theoretical value by the Wenzel equation (~124°), it suggests that water wetted almost the entire surface instead of being supported by sharp tips. The initial radius of a water droplet on Nanopost-Low was ~1 mm, which would create the Laplace pressure of $\Delta P \cong 150$ Pa. On the basis of the criteria discussed in eqs 1 and 2, the pitch (230 nm) and height (~100 nm) of the structures on Nanopost-Low are regarded to be dense and tall enough, respectively, to sustain a dewetted (Cassie) state. However, the cone angle α of the structures is speculated to be too large to sustain the meniscus (i.e., $\theta_A - \alpha < 90°$). During evaporation, the contact angle continuously decreased until 120 min, then reached almost the same angle (111 ± 1°) as that on Smooth (110 ± 2°) and remained unchanged until complete evaporation (Figure 5a). A contact diameter on Nanopost-Low was not changed for the initial 30 min, indicating that the contact line of the droplet was pinned (Figure 5b). Afterward, the contact diameter decreased continuously until complete evaporation. The result suggests that in 30 min (~124°) the inward interfacial tension by the solid−liquid interface became greater than the total outward interfacial tension by the liquid−gas and solid−gas interfaces, creating the continual depinning of the contact line.

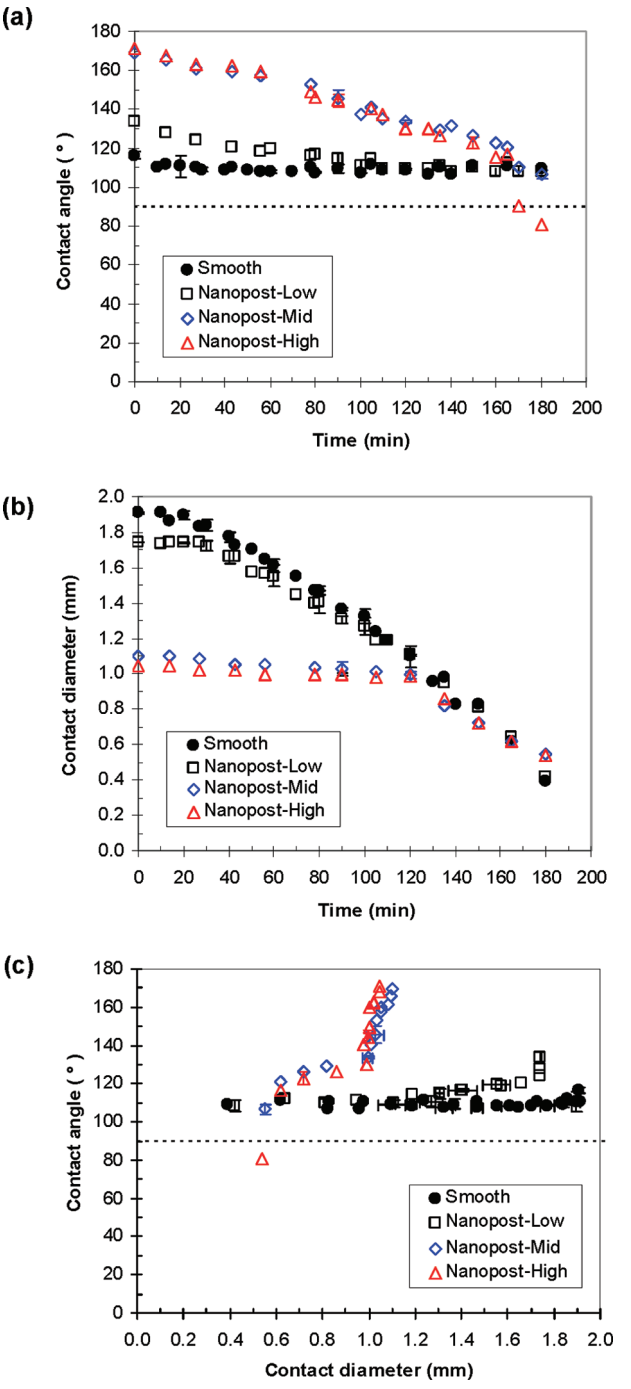

Figure 5. Analysis of captured images for water droplets: (a) change of contact angle over time; (b) change of contact diameter over time; (c) change of contact angle with respect to contact diameter. For the data, average values from three experiments are shown with standard deviation error bars.

On Nanopost-Mid (◇ in Figure 5) and Nanopost-High (△ in Figure 5), the initial contact angles were ~170° for both (Figure 5a), indicating that a water droplet was supported only by the structural tips. Both cases agree well with the theoretical contact angle (173°) expected by the Cassie−Baxter equation with the solid−liquid fraction of $f_{SL} = 0.013$. It shows that, in addition to the structural height and pitch, the cone angle α for the structures of Nanopost-Mid and Nanopost-High were in an allowable range to sustain the dewetted state (i.e., $\theta_A - \alpha > 90°$). During evaporation, the contact angles on both samples continued to decrease to ~120° for 165 min (Figure 5a). In

180 min (just before complete evaporation), the contact angles rapidly dropped, which was more pronounced on Nanopost-High (~80°) than on Nanopost-Mid. In contrast to Smooth and Nanopost-Low, the contact diameters on Nanopost-Mid and Nanopost-High decreased in a much slower pace until 120 min, when the decrease accelerated (Figure 5b). It shows that the contact line of a water droplet on sufficiently tall nanoposts mostly maintained a pinned state on top of the structure tips until a contact angle was reduced to a certain critical angle (e.g., ~135° and ~130° for Nanopost-Mid and Nanopost-High, respectively, for 120 min) (Figure 5c). If the contact angle decreases below the critical angle, the solid−liquid interfacial tension (inward to a droplet) on the structure tip will become greater than the total interfacial tension (outward to a droplet) by the liquid−gas and solid−gas interfaces so that the contact line may retreat easily from tip to tip. The abrupt decrease of a contact angle in 180 min (Figure 5a), especially on Nanopost-High, indicates that a water droplet was collapsed to a Wenzel state, wetting the entire surface. As discussed earlier, the Laplace pressure increases linearly with the droplet curvature. The impalement of the evaporating droplet from a Cassie to a Wenzel state due to such an effect has been reported experimentally[20−23,25] and numerically.[34] On Nanopost-Mid and Nanopost-High in 180 min, the estimated radius of curvature of a water droplet was ~0.3 mm, of which Laplace pressure is expected to be $\Delta P \cong 500$ Pa. According to the criteria of eqs 1 and 2, such a transition due to a pronounced Laplace pressure is not expected for the Nanopost-Mid or Nanopost-High for the given droplet size. After complete evaporation, we frequently observed a small water mark (~0.5 mm in diameter) left on almost all samples. We speculate that the water mark was due to some impurities (e.g., minerals) introduced from the environment during the long (more than 3 h) evaporation process, degrading the original surface hydrophobicity and accelerating the transition to a Wenzel state.

Evaporation of a DMEM Droplet. Figure 6 is a set (i.e., one of the three repeated tests) of the captured images of DMEM droplets during evolution. From all three sets of the captured images, the contact angle and the contact diameter of the evaporating droplets were measured, as presented in Figure 7.

On Smooth (● in Figure 7), an initial contact angle was ~111° (Figure 7a), which is a little bit smaller than the contact angle of a water droplet (~116°). The initial contact angle (~111°) continuously decreased down to almost 0° with a relatively high decrease rate. Meanwhile, a contact diameter was almost unchanged throughout evaporation (Figure 7b), indicating a strong pinning of a contact line. Compared to a water droplet exhibiting an almost constant receding contact angle (110 ± 2°) in retreat, the constant contact-line pinning observed in a DMEM droplet suggests that the original Teflon surface hydrophobicity was degraded by protein adsorption. The increase of pinning corresponds to the increase of contact angle hysteresis, which is attributed to the decrease in receding contact angle with respect to the increased protein concentration in the evaporating droplet and the protein adsorption in the receding area.[35] The protein adsorption would also be facilitated by a capillary flow[36] in which the pinning of the drying DMEM droplet would ensure that liquid evaporating from the edge is replenished by the liquid from the interior. The resulting outward flow would carry the proteins in DMEM to the outer edge, further promoting the protein adsorption.

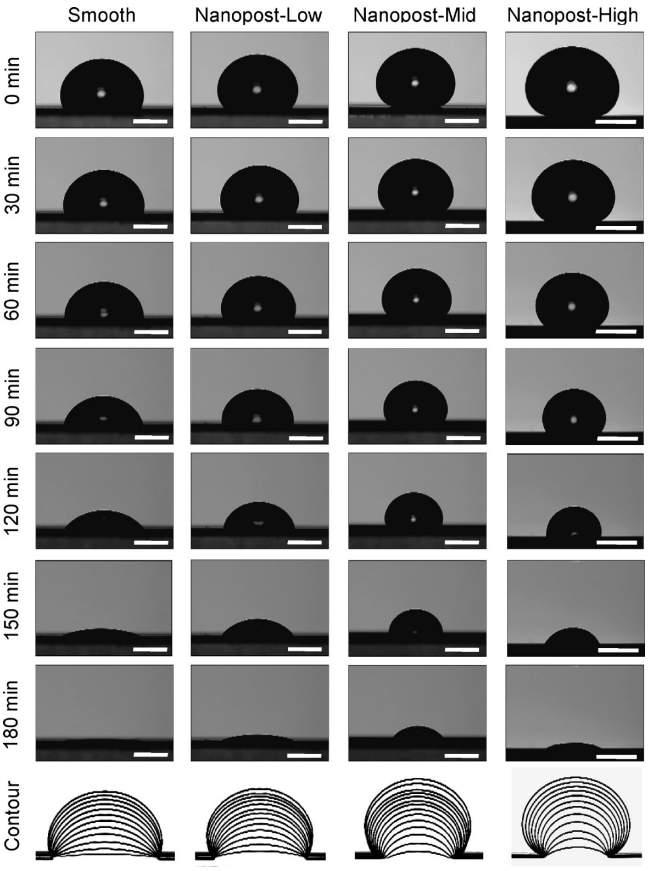

Figure 6. Evaporation of DMEM droplets. Images of droplets (initial volume of ~25 μL) were taken over time in a room environment on smooth and nanopost samples. From the images, the evolution of a contact angle and a contact diameter were measured. The images are shown here for every 30 min. Each scale bar indicates 1 mm. Contours of the droplets were captured by image analysis and drawn overlapping to show the evolution.

On Nanopost-Low (□ in Figure 7), a contact angle started at a little higher value (~124°) than that on Smooth (~111°) (Figure 7a), although still smaller than that with a water droplet (~133°). If the initial contact angle (111°) on Smooth is used as a referential contact angle θ_0 with the same solid−liquid fraction and surface roughness factor as those in water (i.e., $f_{SL} = 0.013$ and $R_f = 1.28$), the theoretical contact angles estimated by the Cassie and the Wenzel equations are 172° and 117°, respectively. Although the initial contact angle on Nanopost-Low (~124°) was slightly larger than the theoretical value by the Wenzel equation (~117°), it indicates that the DMEM wetted almost the entire surface with little air retained (Wenzel state) rather than being supported by sharp tips (Cassie state). Analogous to the case of water, it suggests that the cone angle α of the Nanopost-Low structures was too large to sustain the dewetted state for DMEM (i.e., $\theta_A - \alpha < 90°$), although the structural pitch and height were within the stable conditions for the dewetted state. During evaporation, the contact angle continuously decreased throughout evaporation with a decrease rate close to that on Smooth. Except for a slight increase (~4% from the initial value) for the initial 30 min, the contact diameter remained unchanged afterward (Figure 7b), indicating a strong contact-line pinning throughout the evaporation process due to the protein adsorption. The initial increase of the contact diameter suggests that the protein propagated toward the intact outer nanostructured surface, causing the expansion of the contact line.

(34) Kasumaatmaja, H.; Blow, M. L.; Dupuis, A.; Yeomans, J. M. *Eur. Phys. Lett.* **2008**, *81*, 36003.
(35) Berejnov, V. *J. Colloid Interface Sci.* **2008**, *322*, 246−251.
(36) Deegan, R. D.; Bakajin, O.; Dupont, T. F.; Huber, G.; Nagel, S. R.; Witten, T. A. *Nature* **1997**, *389*, 827−829.

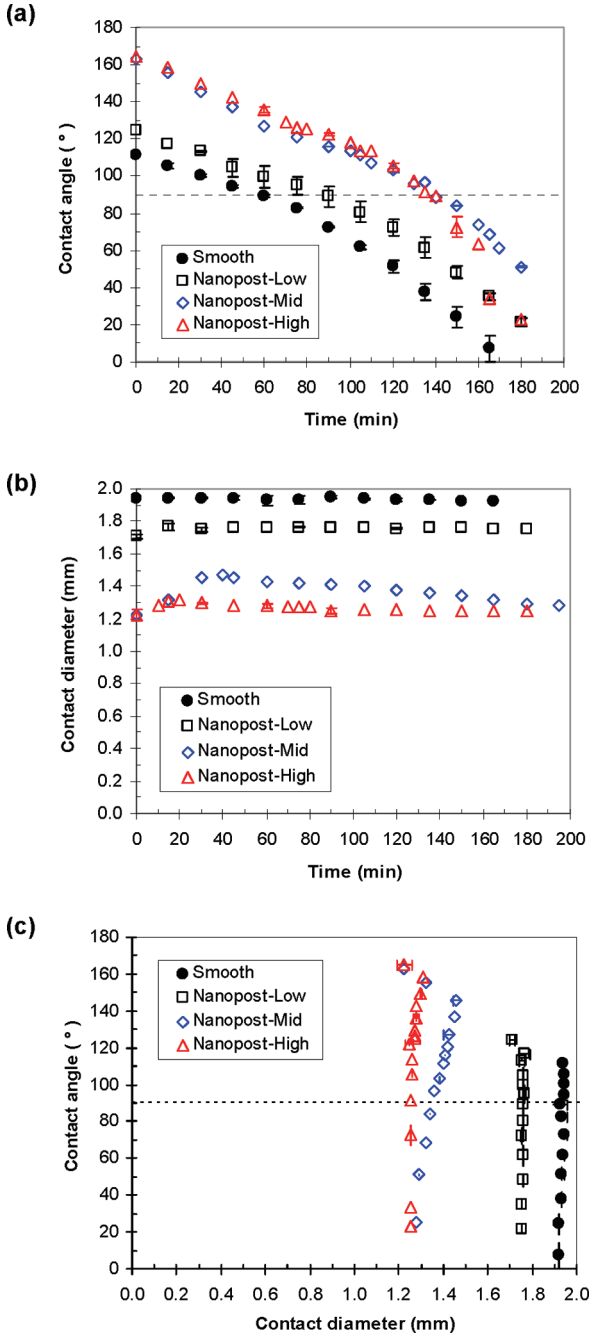

Figure 7. Analysis of captured images for DMEM droplets: (a) change of contact angle over time; (b) change of contact diameter over time; (c) change of contact angle with respect to contact diameter. For the data, average values from three experiments are shown with standard deviation error bars.

On Nanopost-Mid (◇ in Figure 7) and Nanopost-High (△ in Figure 7), initial contact angles were ~163° and ~165°, respectively (Figure 7a), a little bit smaller than the theoretical one (172°) expected by the Cassie−Baxter equation with f_{SL} = 0.013 and θ_0 = 111°. The almost identical contact angles, despite the different structural heights, indicate that the DMEM droplets were resting only on the structural tips (i.e., Cassie state). Similar to the case of pure water, the above result also suggests that the cone angle α for the Nanopost-Mid and Nanopost-High structures was in an allowable range to sustain the dewetted state for DMEM (i.e., $\theta_A - \alpha > 90°$). During evaporation, the contact angle on Nanopost-Mid continued to decrease until complete evaporation at a similar decrease rate to those on Smooth and Nanopost-Low. In the mean time, a contact diameter on Nanopost-Mid increased (~19% from the initial value) until ~30 min and then decreased slowly until complete evaporation, when the diameter became almost the size of the initial state (Figure 7b). It is speculated that the gradual transition from the initial Cassie state on Nanopost-Mid to a Wenzel state during the first ~30 min, causing the increase in the contact diameter, is due to the protein propagation and adsorption onto the nanostructured surface. The measured contact angle in 30 min on Nanopost-Mid was ~145°, agreeing reasonably with the theoretical angle of ~140° expected by the Wenzel equation with h = 300 nm (i.e., R_f = 2.12) and θ_0 = 111°. On Nanopost-High, while the contact angle continued to decrease at almost the same pace as that on Nanopost-Mid until 120 min, it decreased more rapidly afterward until 160 min, and then the decrease rate became mitigated to be similar to those of the other samples. A contact diameter on Nanpost-High increased slightly (~5% from the initial value) until 15 min and then decreased slowly until complete evaporation, when the diameter became the same as the initial state (Figure 7b). The abrupt decrease of a contact angle in 120−160 min and the relatively insignificant increase of a contact diameter compared to that on Nanopost-Mid indicate that the transition from the Cassie to a Wenzel state was prolonged and that the critical transition occurred at a later evaporation stage (e.g., after 160 min). We interpret that it took more time for the proteins in DMEM to propagate and adsorb onto the entire nanostructures underneath a droplet and make the surface fully wet, since the structure of Nanopost-High was taller than that of Nanopost-Mid (~500 nm vs ~300 nm). While the DMEM droplets exhibited the distinct evaporation evolution in terms of contact angle and diameter depending on the structural height, the final contact diameters after complete evaporation are almost the same between the two (Figure 7b). Although a noticeable change (especially initial increase) of contact diameter was observed in both samples, the changes were much less than those with water, suggesting that the prominent pinning effect of a contact line was due to the modified surface wettability by the protein adsorption.

One of the potential applications of superhydrophobic surfaces is the prevention of biofouling.[37,38] The main object of such applications is to use the air barrier on the surface to minimize the contact of biofoulers, such as cells and proteins, on the solid surface. For this purpose, it is critical to maintain the Cassie state. Another application is biomedical engineering. Superhydrophobic surfaces affect the protein adsorption and cell adhesion,[39,40] which are important in implantable biomedical devices and tissue engineering. Cells *in vivo* involve a liquid environment containing various proteins. For typical *in vitro* cell tests, the DMEM is used for the liquid environment. In this paper, the cell culture medium was selected as a complex fluid to study the effects of the biofouler (proteins) on the droplet evaporation and the wetting transition. The cell culture medium cannot be considered a well-controlled complex fluid so that the deeper understanding on the surface phenomena such as adsorption and pinning at the nanoscale interface could not be directly measured in this study. However, the indirect estimation of the droplet evaporation and wetting

(37) Carman, M. L.; Estes, T. G.; Feinberg, A. W; Schumacher, J. F., Wilkerson, W.; Wilson, L. H.; Callow, M. E.; Callow, J. A.; Brennan, A. B. *Biofouling* **2006**, *22*, 11−21.
(38) Genzer, J.; Efimenko, K. *Biofouling* **2006**, *22*, 339−360.
(39) Koc, Y.; de Mello, A. J.; McHale, G.; Newton, M. I.; Roach, P.; Shirtcliffe, N. J. *Lab Chip* **2008**, *8*, 582−586.
(40) Leibner, E. S.; Barnthip, N.; Chen, W..; Baumrucker, C. R.; Badding, J. V.; Pishko, M.; Vogler, E. A. *Acta Biomater.* **2009**, *5*, 1389−1398.

phenomena by measuring contact angle and contact line dynamics in well-controlled evaporative environment showed the effects of proteins on the nanoscale interface phenomena such as spreading and pinning of evaporating droplets.

5. Summary and Conclusions

In contrast to the superhydrophobic surfaces consisting of microscale structures or random patterns as previously tested by others, we investigated droplet evaporation on well-ordered nanoscale structures. Particularly, the tested nanostructures had sharp tips and a fixed pitch but three different heights. The sharp tip was to maximize the initial surface superhydrophobicity, and the varying heights were to study the effect of the nanotopographical three-dimensionalities on the evaporation process of droplets such as the dynamics of a contact angle and a contact diameter.

We investigated the evaporation processes of two different liquids—pure water and a protein solution of cell culture media. Short nanopost structures with a gradual slope did not exhibit superhydrophobicity, following a wetting (Wenzel) state. In contrast, tall nanostructures with a steep slope exhibited great superhydrophobicity, following a dewetting (Cassie) state independent of the structural heights. In the evaporation of water, the droplet on the tall nanostructures maintained the dewetted state throughout the evaporation with two distinctive stages: an initial pinning stage of an almost constant contact diameter and the remainder a slip-and-jump stage of continuous decrease in the contact diameter. In the evaporation of a protein solution, which is typically known to foul hydrophobic surfaces, the droplets on the smooth and nanostructured samples all showed strong pinning of a contact line throughout the evaporation. Although a noticeable increase of contact diameter was observed on nanostructured surfaces, especially in the early evaporation stage, the contact diameter (or area) still remained much smaller than that on a smooth surface due to the initial surface superhydrophobicity. This phenomenon is useful for some biological applications, e.g., a given droplet volume on a smaller contact area throughout the evaporation would leave more concentrated DNA or protein on a surface.[41]

In conclusion, our results demonstrated that not all the hydrophobic surface structures exhibit superhydrophobicity for droplets, illustrating that the structural three-dimensionality and the effect of complex fluids such as protein adsorption in biological solutions are important factors influencing the initial and continual superhydrophobicity of evaporating droplets.

Acknowledgment. This work has been supported by the National Science Foundation Nanoscale Interdisciplinary Research Teams Grant 0103562.

(41) Ressine, A.; Marko-Varga, G.; Laurell, T. *Biotechnol. Annu. Rev.* **2007**, *13*, 149−200.